



January 2007

Volume 3 Issue 4-6

Trade Science Inc.

# Analytical CHEMISTRY

An Indian Journal

Full Paper

ACAIJ, 3(4-6), 2007 [161-171]

## Spectrochemical Analysis Of Spatially And Temporally Resolved Laser Induced Aluminum Plasma



Corresponding Author

M.A.Harith  
National Institute of Laser Enhanced Sciences  
(NILES), Cairo University, (EGYPT)  
E-Mail: mharithm@niles.edu.eg



Co-Authors

H.Imam, V.Palleschi  
IPCF/CNR, Applied Laser Spectroscopy Laboratory,  
Pisa, (ITALY)

Received: 7<sup>th</sup> October, 2006

Accepted: 22<sup>nd</sup> October, 2006

Web Publication Date : 21<sup>st</sup> December, 2006

### ABSTRACT

In the present paper a detailed spectrochemical investigation of the temporal and spatial evolution of the plasma produced by interaction of Q-switched Nd: YAG laser pulses at 532 nm with pure aluminum target is performed via optical emission spectroscopy (OES) in vacuum ( $10^{-5}$  torr). Comparison of the spectra taken at different distances from the target surface facilitates discussing fundamental concepts of the laser induced plasma (LIP). Such measurements have been exploited to understand the main processes involved and must be taken into account for the analysis of this kind of plasma. The LIP mean expansion velocity has been determined by measuring the ionic emission temporal profiles usually referred to as the time of flight (TOF) profiles. The temporal behavior of the spectral emission has been explained and interpreted in view of the three body recombination processes. Problems concerning the existence of and departure from the local thermodynamic equilibrium (LTE) in the LIP are studied carefully as observed in the performed experiment.

INDIA

© 2007 Trade Science Inc. -

### KEYWORDS

Spectrochemical analysis;  
LIPS;  
Temporally and spatially  
resolved spectra;  
Local thermodynamic  
equilibrium;  
Time of flight.

### INTRODUCTION

Besides its potential as a powerful spectro-chemical analytical technique, study of the laser induced plasma (LIP) plays a fundamental role for diagnostic purposes in many applications concerning laser-matter interaction. During the last few years many works

have been published and four international conferences have been held concerning this issue<sup>[1-4]</sup>. The phenomenology of energy transport mechanisms encountered in the interaction of laser with solid targets consists of four different stages: the laser ablation of the target; plasma generation; laser interaction with the plasma and plasma expansion. The ini-

## Full Paper

tiated expanding atomic plasma at high temperature (6000 - 20000 K), is ionized by the inverse bremsstrahlung and the photoionization processes, expanding rapidly (approximately at  $10^6$  cm/s) perpendicularly to the target surface<sup>[5]</sup>. During the expansion, the main mechanism of transition of bound electrons from the lower levels to the upper levels and vice versa is driven by inelastic collisions of electrons with heavy particles, while the concentration of charged particles is controlled by the electron impact ionization and three - body recombination of electrons with ions. Radiative processes such as re-absorption, spontaneous and stimulated emission are also important in determining the concentration of emitting levels<sup>[6]</sup>. The study of laser induced plasma is based on the assumption of local thermodynamic equilibrium (LTE) and optically thin plasma<sup>[7]</sup>. In LTE the Maxwell, Boltzmann and Saha relations are still valid locally, so the electron density, temperature and chemical composition can be easily determined. For the LTE condition to hold, only small variations of the system are admitted so that the times associated to the establishment of kinetic balances are smaller than that of the plasma variations<sup>[8]</sup>. In fact, this scenario belongs to thermal plasma in stationary conditions. In low of pressure ( $10^{-5}$  torr), LIP expanding with supersonic velocity ( $10^5$ - $10^7$  cm/s), so the plasma parameters can change in such very short time of expansion compared with the time necessary for the establishment balance among elementary processes. This expansion might also results in a departure from LTE. This could be an important point of our study to find out whether the conditions of LTE are satisfied or not in the plasma formation during the expansion phase.

The strong interest in laser induced plasma applications has been leading the development of many experimental techniques to characterize laser ablation plasmas<sup>[9]</sup>. Among them the most convenient technique, especially for the investigation of the initial stages of LIP, is the optical emission spectroscopy (OES)<sup>[10, 11]</sup>. Since OES is based on the study of the spectral intensity and broadening of lines, the intrinsic light emission of the LIP and does not need any other excitation sources or intrusive systems, the experimental set-up is very simple and adaptable to

automation and remote sensing<sup>[12-14]</sup>.

In the present work, detailed experimental and theoretical study of the dynamics of pure aluminum laser induced plasma in vacuum will be presented. Plasma parameters and composition will be studied spatially and temporally via OES technique. The time of flight (TOF) technique will be exploited to investigate the expansion regimes of LIP in vacuum. The obtained results will be modeled in order to understand different processes involved in the LIP evolution and expansion.

## EXPERIMENTAL

The schematic diagram of the experimental arrangement used for the experimental part of this work is depicted in figure 1. It consists of a Q-switched Nd: YAG laser (Continuum NY 81-30), a vacuum chamber, a pumping system and an optical emission spectroscopy system.

Laser induced plasma has been produced by focusing the second harmonic (532 nm) of the Nd:YAG laser (100 mJ, 8 ns, and 1 Hz) via a quartz lens of 20-cm focal length onto the target surface. The polished high purity aluminum (99.9999%) target was positioned into the vacuum chamber, which was pumped out up to  $10^{-5}$  mbar by rotary and turbo molecular pumps. The target holder was rotated around an axis parallel to the laser beam between shots, to allow sampling from fresh locations on the target surface and avoiding formation of deep craters, thus improving the reproducibility and accu-

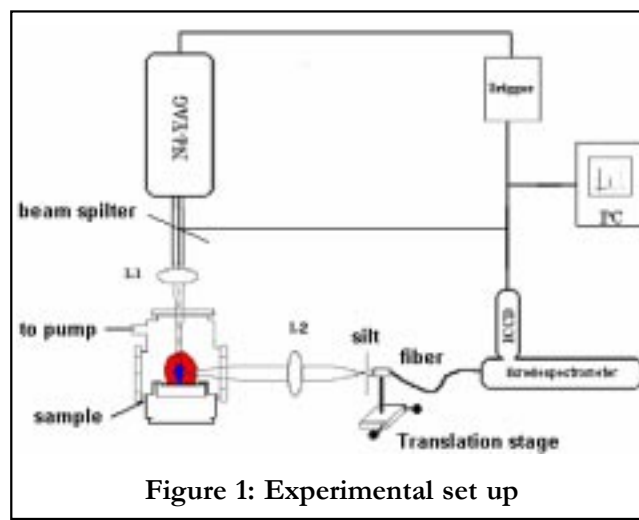


Figure 1: Experimental set up

racy of spectral emission. The plasma emission was collected by a 15cm focal length lens to make a virtual image 1:1 on the optical fiber entrance. The quartz optical fiber used has an aperture of 600 $\mu$ m diameter, and mounted on an x-y micro-translation stage. The aperture of the optical fiber was aligned with the centerline of the plume to ensure that the emission signal was collected perpendicularly with respect to its symmetry axis. The input of the optical fiber was coupled to a slit of 120 mm width for obtaining an effective spatial resolution of 150 mm. The output of the optical fiber was connected to the echell spectrometer (Mechelle 7500) coupled to an intensified charge couple device, ICCD, (DiCAM, Optics, Germany), allowing simultaneous spectral analysis in the range 200 - 900 nm with a constant spectral resolution  $\lambda/\Delta\lambda=7500$ .

The gate width (2  $\mu$ s for all measurements) and delay time for the spectroscopic data acquisition were controlled by computer. To optimize the signal-to-noise ratio and spectra reproducibility, the acquisition of the spectra was carried out by averaging 50 single accumulated spectra. To investigate the spectral contour and width of the spectral lines the in-

strumental line shape function of the optical system was measured using the emission lines of a mercury lamp and He-Ne laser.

The analysis of the emission spectra was accomplished using the commercial 2D/ and 3D/GRAMS/32 software.

The plasma emission spectrum was recorded at several distances from the target surface while varying the delay time from 0 to 300 ns.

Thus, spatially and temporally resolved optical emission spectroscopy is used to investigate the evolution of the spectral lines intensity and broadening, and to estimate temperature and electron density as a function of time and distance from the target surface (0-2mm).

## RESULTS AND DISCUSSION

### Optical emission spectroscopy of pure Al target

The emission spectra of LIP have been observed at different distances from the target surface along the LIP propagation axis and after different delay times from the laser pulse. By varying the position

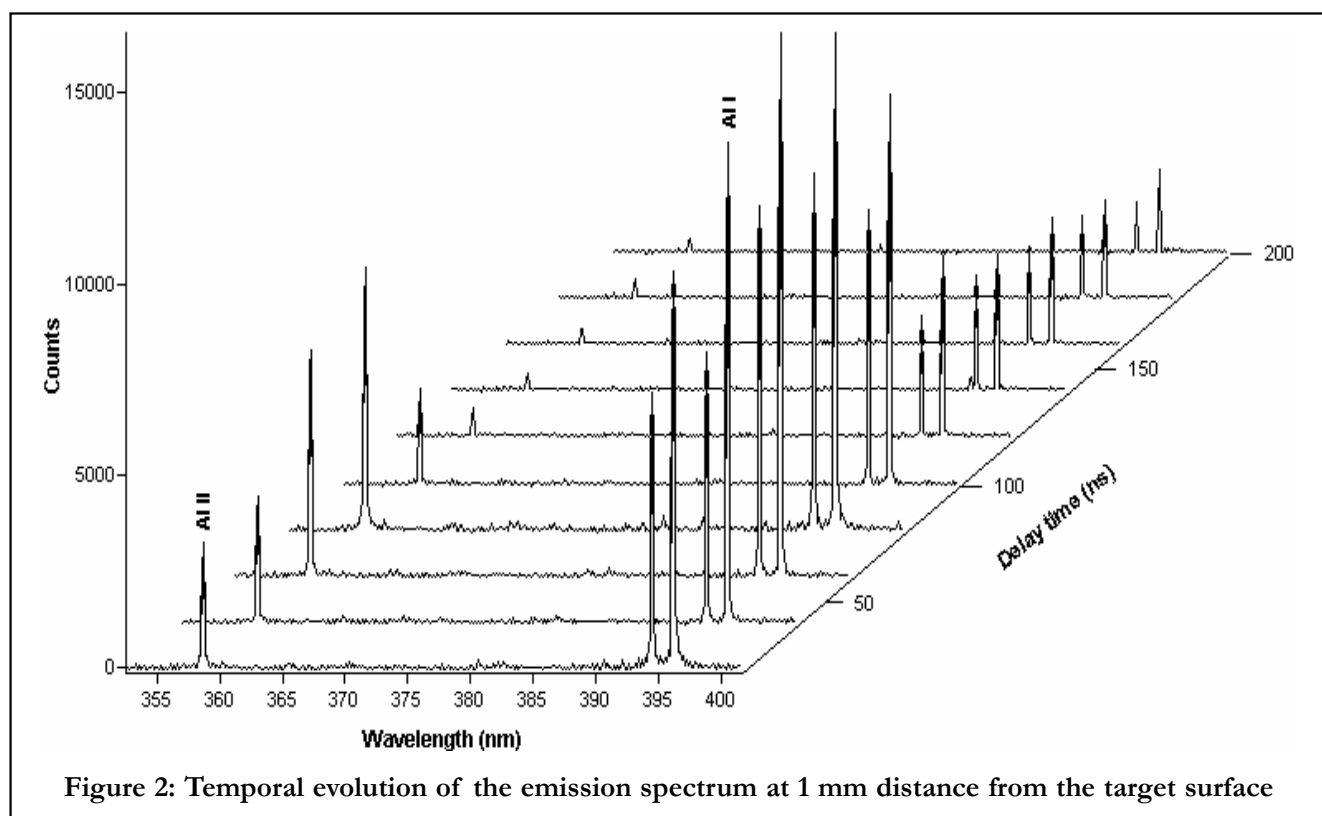


Figure 2: Temporal evolution of the emission spectrum at 1 mm distance from the target surface

## Full Paper

of the optical axis of the collecting optics with respect to the target surface, spatially resolved spectra have been obtained that include many neutral and ionized emission lines of the aluminum plasma. From figure 2 it is clear that the maximum intensity of the spectral lines is reached after a characteristic time, depending on the observation distance, and it represents the most populated section of LIP. Such maximum value of the lines intensity maximum is reached when the core of the expanding plasma passes in front of the optical collection system. Depending on the observation distance (with respect to the target surface) the first stage in temporal distribution of the spectra shows a regime where the ionic lines are more intense than the atomic lines. However, on

the tail of the temporal distribution - corresponding to the colder part of the plasma - the ionic lines disappear.

Al I (neutral aluminum) at 305 nm and Al II (ionized aluminum) at 281.6 nm have been chosen for the spectral analysis as shown in figure 3. The transitions of these two emission lines have high lower energy levels and small transition probabilities, which strongly lowers the possibility of their self-absorption in the colder parts of the plasma.

From the temporal and spatial distributions of the line intensities at 305 nm and 281.6 nm, represented in figure 3, we can observe that Al II emission is confined to a narrower region than Al I emission, corresponding to regions of higher temperature in which the ionization process is enhanced during the expansion process of the plasma. A similar distribution for atomic and ionic lines in plasma was found by Sdorra and Niemax<sup>[6]</sup>.

### Time of flight (TOF) measurements

The optical emission spectroscopy (OES) is the simplest way to perform TOF measurements in the bright region of LIP (0-2 mm). Study of LIP species evolution has been carried out by temporally and spatially resolved OES at different distances from the surface of the target. As mentioned before, the two non-resonance lines with high emission coefficients and high lower energy levels, namely Al I at 305 nm and Al II at 281.6 nm, have been used for the TOF measurements. For the determination of the expansion mean velocity we considered the ionic emission line because the time of flight of the atomic emission line can present an additional delay due to the three body recombination, as will be explained later

Figure 4 shows the normalized TOF of Al II species. By measuring the shift of the peaks of time of flight (TOF) for each distance it is possible to obtain the mean velocities of the LIP along the propagation axis. The corresponding results are shown in figure 5a and 5b for the expansion.

In the range of distances investigated experimentally, the velocity of LIP increases with the distance. This trend of LIP velocity is due to the acceleration of the ablated particles from the initial velocity  $v_0 =$

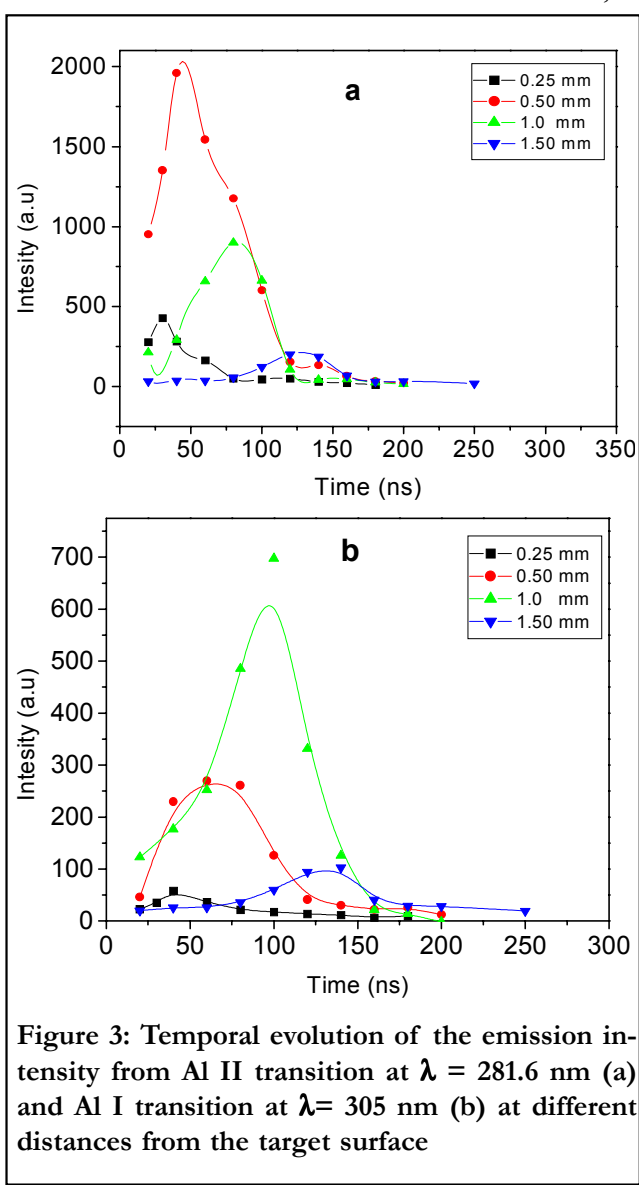


**Figure 3:** Temporal evolution of the emission intensity from Al II transition at  $\lambda = 281.6$  nm (a) and Al I transition at  $\lambda = 305$  nm (b) at different distances from the target surface

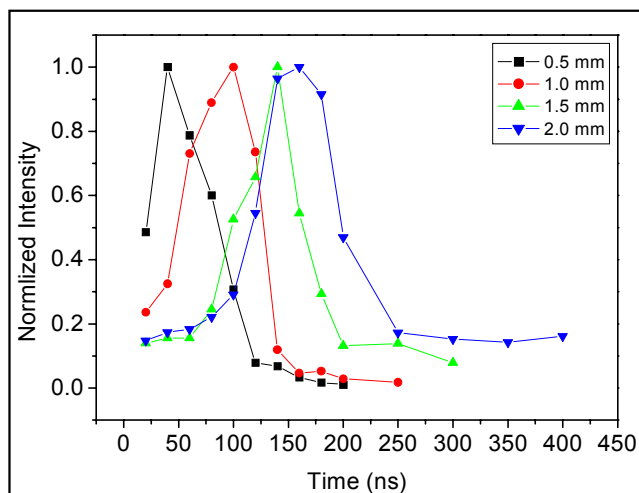


Figure 4: TOF profiles of Al II emission intensities at different distances from the target

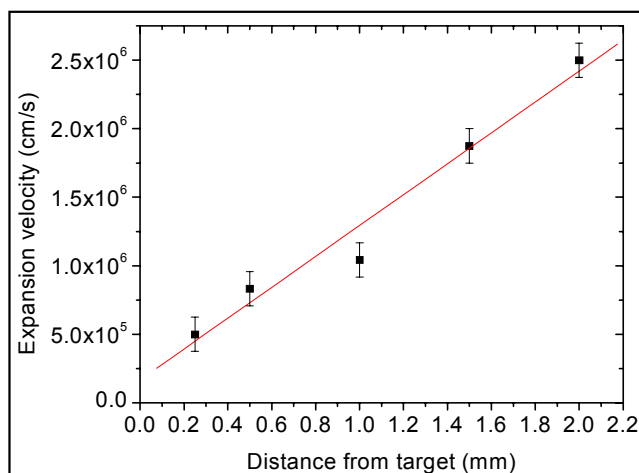


Figure 5a: Position of the TOF peak at different times

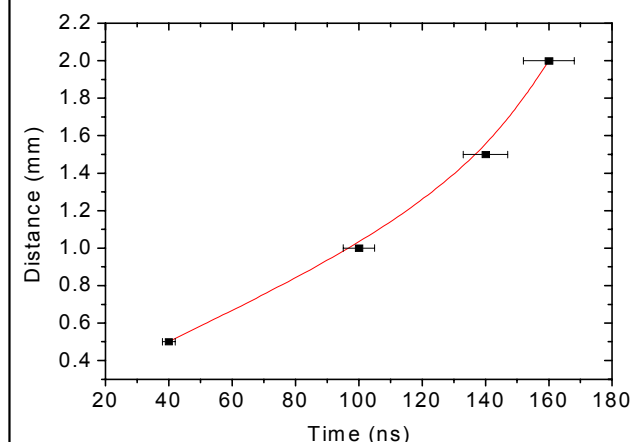


Figure 5b: Expansion velocity of the plume as a function of the distance from the target

0 before the laser pulse energy reaches the ablation threshold, to a maximum velocity  $v_{\max}$  that is probably reached not far from the maximum distance here considered (2 mm). Then the velocity decreases, since part of the energy is expended in intra-plume collisions and in moving and heating the residual buffer gas<sup>[5]</sup>.

### Determination of the electron density

One of the most powerful spectroscopic techniques to determine the electron density with reasonable accuracy is the measurement of the Stark broadening profile of the atomic emission lines. In the present experiment, the Al II transition at 281.6 nm [ $4s^1S(0) - 3p^1P^0(1)$ ] has been chosen for the electron density measurements.

The FWHM of the Stark broadened lines  $\Delta\lambda_{1/2}$  is related to the electron density by the expression (for singly ionized ions)<sup>[17]</sup>:

$$\Delta\lambda_{1/2} = 2w \left( \frac{N_e}{10^{16}} \right) + 3.5A \left( \frac{N_e}{10^{16}} \right)^{1/4} \left( 1 - 1.2N_D^{-1/3} \right) w \left( \frac{N_e}{10^{16}} \right) \text{Å} \quad (1)$$

The first term in Eq. (1) gives the contribution from electron broadening, and the second term is the ion broadening correction.  $w$  is the electron impact parameter, which can be interpolated at different temperatures, and  $A$  is the ion broadening parameter. Both  $w$  and  $A$  are weak functions of temperature.  $N_e$  is the electron density ( $\text{cm}^{-3}$ ) and  $N_D$  the number of particles in the Debye sphere.

The contribution from quasi-static ion broadening (the second term of Eq. (1)) is small in our case. Its value can be evaluated from the extrapolation of the Griem estimation for  $A$  and  $w$  (for  $T_e = 8000$  K and  $N_e \sim 10^{17} \text{ cm}^{-3}$ , its contribution is less than 2%)<sup>[17]</sup>. Neglecting this contribution, equation (1) can be reduced to:

$$\Delta\lambda_{1/2} = 2w \left( \frac{N_e}{10^{16}} \right) \text{Å} \quad (2)$$

The temporal evolution of  $N_e$  is found to diminish exponentially with time and then level off, taking into account an experimental error of about 15%. The fast decay rate of electron density can be attributed to the plasma expansion, while the slowing and

## Full Paper

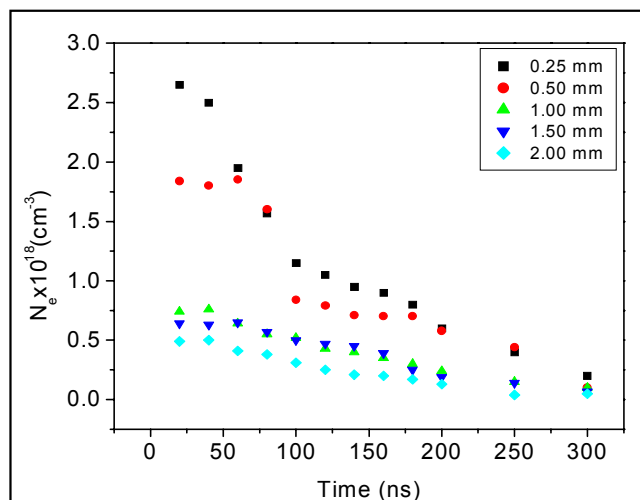


Figure 6: Electron density temporal evolution ( $N_e$ ) at different distances from the target

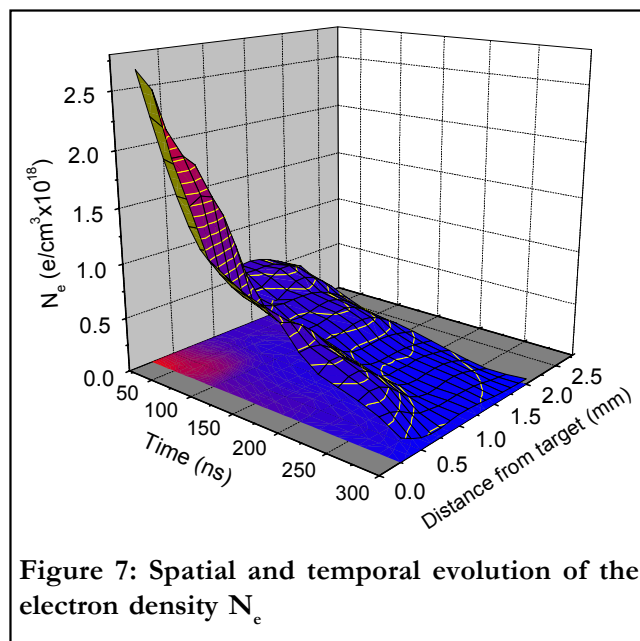


Figure 7: Spatial and temporal evolution of the electron density  $N_e$

leveling off at longer times are probably due to recombination as shown in figure 6.

From figure 7 it is clear that the highest value of the electron density is reached close to the target surface, and then it decreases at longer times and distances from the target. It is also noticeable that the temporal behavior of the electron density is the same at all different distances away from the target surface.

### The three-body recombination effect on the temporal line profile

Inspecting figure 8, it is observable that the TOF

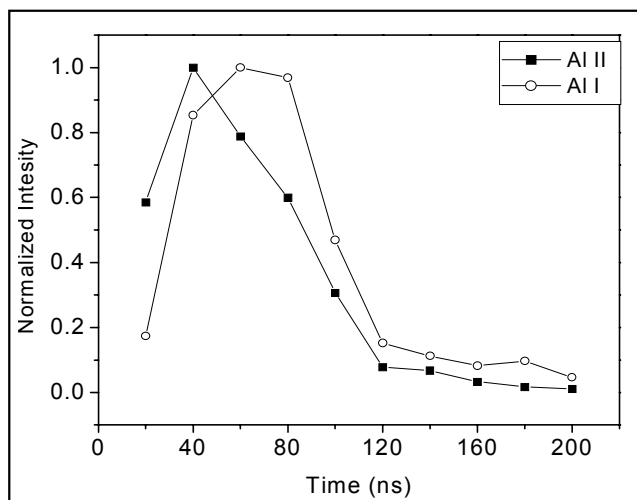


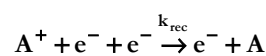
Figure 8: Comparison of normalized TOF curves of Al I and Al II at 0.5 mm from the target surface

peak corresponding to the Al I is time shifted with respect to those of the Al II. This delay could be attributed to the three-body recombination mechanism. Additional amount of neutral atoms produced by the recombination of ions and electrons leads, in fact, to such apparent delay between Al I and Al II TOF maxima.

During the evolution of the plasma plume, several processes take place that change the relative concentration of the species within the plume. Immediately after the end of the laser pulse, the main mechanism that sustains the ionization process in the plasma is the collisional ionization of neutral atoms by the fast electrons in the plume. This mechanism of ionization can be represented as



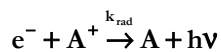
This equation represents the process where a high-energy electron collides with a neutral atom  $A$ , producing, with probability  $k_{\text{ion}}$ , an ionized atom  $A^+$  and another free electron which, in turns, may ionize other neutral atoms through the same process. The reciprocal process of electron-impact ionization is called three-body recombination, and may be represented as



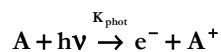
In this process, in the presence of a second electron one free electron is captured by an ionized atom,

resulting in the production, with probability  $k_{\text{rec}}$ , of a neutral atom A.

Direct radiative recombination is also possible



as well as the inverse process



which is just the photo-ionization process. Atom-atom and ion-atom collisions can be, in general, neglected assuming that electron-atom collision frequency dominates the kinetics of the reactions.

The above mentioned processes may be considered for deriving the temporal evolution of the electron density and the concentration of the other species in the plasma. Let us now apply the theoretical model to our experimental conditions, i.e. the expansion of pure aluminum plasma in vacuum. In these conditions, assuming that the time variations of the plasma electron density due to the LIP expansion are negligible, the following dynamical equation holds for the electron density:

$$\frac{dN_e}{dt} = k_{\text{ion}} N_e N_{\text{AlI}} - k_{\text{rec}} N_e^2 N_{\text{AlII}} - k_{\text{rad}} N_e N_{\text{AlII}} + k_{\text{phot}} N_e N_{\text{AlI}} \quad (3)$$

where N indicates the concentration ( $\text{cm}^{-3}$ ) of the particles denoted by the subscripts,  $k_{\text{ion}}$  ( $\text{cm}^3\text{s}^{-1}$ ),  $k_{\text{rec}}$  ( $\text{cm}^6\text{s}^{-1}$ ),  $k_{\text{rad}}$  ( $\text{cm}^3\text{s}^{-1}$ ) and  $k_{\text{phot}}$  ( $\text{cm}^3\text{s}^{-1}$ ) are the rate constants of electron-impact ionization, three-body recombination, radiative recombination and photo-ionization, respectively.

Radiative and photo-ionization processes are the dominating processes which occur in the plasma during the laser pulse and immediately after. In fact, such processes are associated with the strong continuum emission which is typical of LIP in its early stage. At longer times, as in our experimental conditions, their influence on the plasma parameters reduces; so that they can be safely neglected. Therefore, considering the plasma neutrality condition  $N_e = N_{\text{AlII}}$ , which holds in the absence of other ionic species that may contribute to the electron density balance, one can rewrite the above equation as:

$$\frac{dN_e}{dt} = k_{\text{ion}} N_e N_{\text{AlI}} - k_{\text{rec}} N_e^3 \quad (4)$$

According to Eq. (4), there are three possible evolution regimes for the electron density

- (1)  $dN_e/dt = 0$  equilibrium condition,
- (2)  $dN_e/dt > 0$  ionization prevails,
- (3)  $dN_e/dt < 0$  recombination prevails.

If  $dN_e/dt \neq 0$ , then ionization ( $dN_e/dt > 0$ ) or recombination ( $dN_e/dt < 0$ ) prevails and departure from equilibrium occurs<sup>[15]</sup>.

To investigate the time evolution of  $N_e$ , it is necessary to take into account that we have to determine the  $N_e$  corresponding to the same section of the plasma. However, the plasma is expanding, so that different parts of the LIP will move to different positions with time. In order to sample the same section of the plasma at different times, we can determine  $N_e$  from the emission spectrum corresponding to the maximum of TOF signal at different distances. We are thus assuming that the maximum TOF signal is produced by the same portion of the plasma when it passes in front of the detector; because of the expansion velocity, this portion of the plasma will move away from the target and will reach the detector at different times as the distance from the target is increased. By collecting the optical spectrum at the maximum of the TOF emission, both  $N_e$  and the corresponding time at which this parameter is measured are known.

Figure 9 depicts  $N_e$  as a function of time; it can

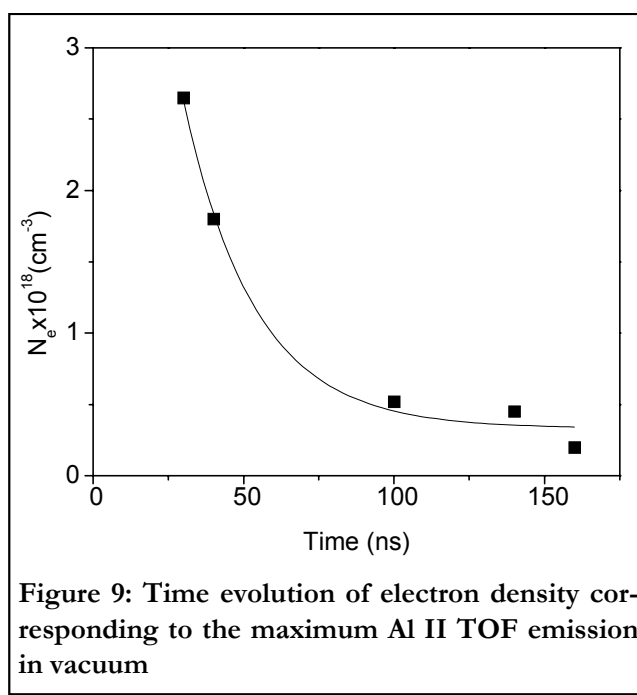


Figure 9: Time evolution of electron density corresponding to the maximum Al II TOF emission in vacuum

## Full Paper

be observed that  $dN_e/dt < 0$ . This means that departure from equilibrium indeed takes place, and there is a predominance of the three-body recombination process over that of electron-impact ionization. On the basis of these observations we can conclude that during the expansion, while the excitation and de-excitation by electron impacts are the main mechanisms that govern the distribution of particles among the excited states, three-body recombination is the main mechanism that governs the concentration of charged particles.

From the fitting of the experimental data with a function obtained from eq. (4), the recombination constant can be estimated as  $k_{\text{rec}} = 0.9 \times 10^{-30} \text{ cm}^6/\text{s}$ , which is in good agreement with the calculated theoretical values reported in the literature ( $k_{\text{rec}} \sim 10^{-30} \text{ cm}^6\text{s}^{-1}$ )<sup>[7]</sup>.

From our experimental data, the temporal dependence of  $k_{\text{rec}}$  can also be obtained. Since the TOF profiles are the result of the velocity distribution of the species and of the kinetic processes, considering the time decay of the TOF signal is possible to estimate the recombination constant directly by the temporal evolution of  $N_e$  for each distance from the target.

The  $N_e$  values have been obtained by Stark broadening for the decay side of the Al II TOF curves between 0.5 and 2 mm. In fact, before the maximum of TOF curves it is not possible to have an exact evaluation of the line contour because of the continuum spectra, as discussed above, while after 2 mm the Stark broadening becomes comparable to the instrumental broadening so that the estimation of  $N_e$  becomes too rough<sup>[18]</sup>. Values of  $dN_e/dt$  are obtained by the exponential fit of the temporal evolution of  $N_e$ , while the second derivative of  $dN_e/dt$  with respect to  $N_e$  is calculated using a polynomial fit. In this case we can use all the experimental measurements after the maximum so that an accurate fitting can be achieved (correlation coefficient  $R > 0.99$ ). The recombination rate constant estimated in this way is again of the order of  $10^{-29} - 10^{-30} \text{ cm}^6\text{s}^{-1}$ , in good agreement with the published data<sup>[7]</sup>. The corresponding values of the three-body recombination rate constant are reported in figure 10.

The recombination time can be estimated by the values of the rate constant of recombination pro-

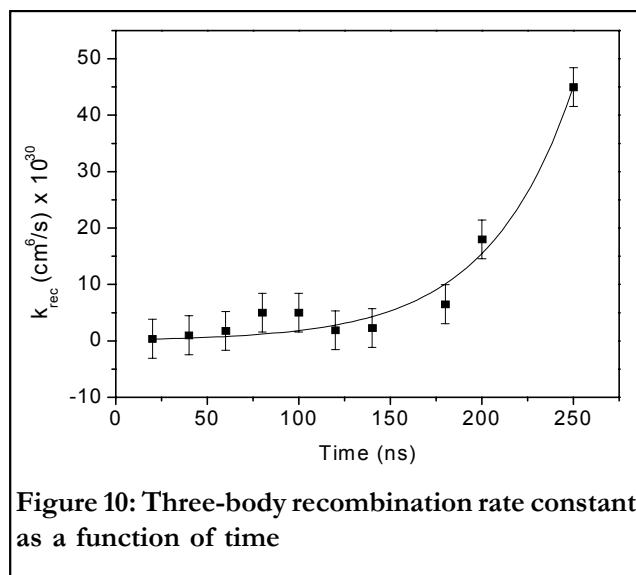


**Figure 10: Three-body recombination rate constant as a function of time**

cess, using the relation  $t_{\text{rec}} = (N_e^2 k_{\text{rec}})^{-1}$  which gives a value of  $t_{\text{rec}} \sim 10^{-7} - 10^{-6} \text{ s}$ . Since the velocity of the plasma expansion is in the range  $10^5 - 10^6 \text{ cm/s}$ , as determined experimentally, and the typical plasma dimensions considered are of the order of 1 mm, we can estimate an expansion time of  $10^{-7} - 10^{-6} \text{ s}$ . We can then conclude that:

$$t_{\text{ion}} > t_{\text{rec}} \sim t_{\text{exp}}$$

As a consequence of the fast expansion of LIP, we can thus establish that the laser-induced aluminum plasma is in a quasi-equilibrium state. The time of expansion is less than the corresponding time for establishment of Saha balance so the plume expands in quasi-equilibrium state and deviation from equilibrium has a recombination character.

### Measurements of the plasma temperature

The plasma temperature can be determined from the relative measured intensities of the emission lines using the well known Boltzmann plot method, provided that the transition probabilities ( $A_{mn}$ ) from a given excitation state are known. For high electron densities, the main mechanism of transition of bound electrons from the lower level to the upper level and vice-versa is inelastic collisions of electrons with heavy particles (in this case Al I and Al II). Therefore the populations of the excited states follow the Boltzmann distribution and the intensity  $I_{mn}$  of the spectral transition line between two bound levels of species  $z$  in plasma is given by:

$$I_{mn} = F \frac{g_m A_{mn}}{\lambda_{mn} U_z(T_z)} N_z \exp\left[-\frac{E_m}{kT_z}\right] \quad (5)$$

By plotting the logarithm of the measured emission intensity of ionic and atomic lines transition of Al as function of the corresponding energy of the upper level, the following equations hold:

$$\ln\left[\frac{I_{mn}\lambda_{mn}}{g_{mn}A_{mn}}\right] = m_z + q_z$$

$$q_z = \ln\left[\frac{N_z}{U_z(T_z)} F\right] \quad m_z = -\frac{1}{kT_z} \quad (6)$$

Where  $I_{mn}$  is the intensity of the light emitted in the transition,  $k$  is the Boltzmann's constant,  $\lambda_{mn}$  is the wavelength of the photons emitted in the transition from the upper excited energy level  $E_m$  to the lower energy level  $E_n$ ,  $U_z$  is the partition function of the species  $z$  calculated at  $T_z$ ,  $N_z$  is the concentration of the species  $z$  in the ground state and  $F$  is an experimental parameter which takes into account the optical efficiency of the collection system as well as the plasma density and volume.

For the evaluation of the plasma temperature via the Boltzmann plot method, it is important to verify that the plasma is not optically thick for the lines used. This was done by checking the ratio of emission intensities of Al II at 281.6 nm, 358.6 nm, 624 nm and 466.3 nm and Al I at 256.8 nm, 257.5 nm, 305nm, 305.7 nm, 308.2 nm, 309.2 nm according to the procedure described by Radziemski et al.<sup>[9]</sup> The intensities were observed to be in a ratio that is consistent with the ratio of their statistical weights, which indicates that the plasma was optically thin for these wavelengths.

The excitation temperature of the LIP was estimated from the emission intensity of the atomic lines (Al I) and ionic lines (Al II) as mentioned above.

Figure 11 (a and b) show Boltzmann plots for Al I and Al II, obtained at 1mm distance from the target surface and the same delay time. The temperature of the species is obtained by the least square linear fit of the experimental data; and its dependence on time, and distance from the target is plotted in figure 12.

Comparing the obtained temperature values, we

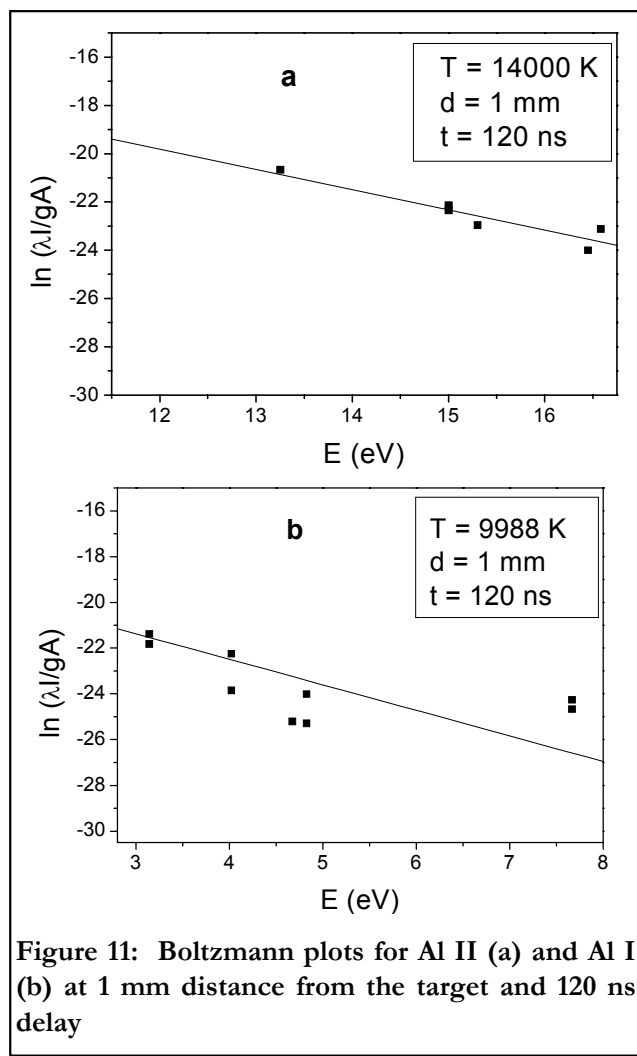


Figure 11: Boltzmann plots for Al II (a) and Al I (b) at 1 mm distance from the target and 120 ns delay

can observe that the temperatures of Al II and Al I are appreciably different. The variation of the temperature of the neutral species is almost insignificant in time, as it changes from 12000 to 8000 K, whereas the temperature of the ionized species decreased from 20000 to 11000 K, as shown in figure 13. The difference between plasma temperatures calculated for the ionic and atomic species in vacuum increases at shorter delay times and at longer distances from the target, as shown in figure 13.

In fact, at shorter times after the onset of the laser-breakdown, the fast dynamics of the plasma does not allow for the system to reach thermodynamic equilibrium, so that the relative concentrations of the different species in the plasma cannot be described with just a single temperature as it should be in the framework of the LTE theory. Moreover, immediately after the onset of the laser break-

## Full Paper

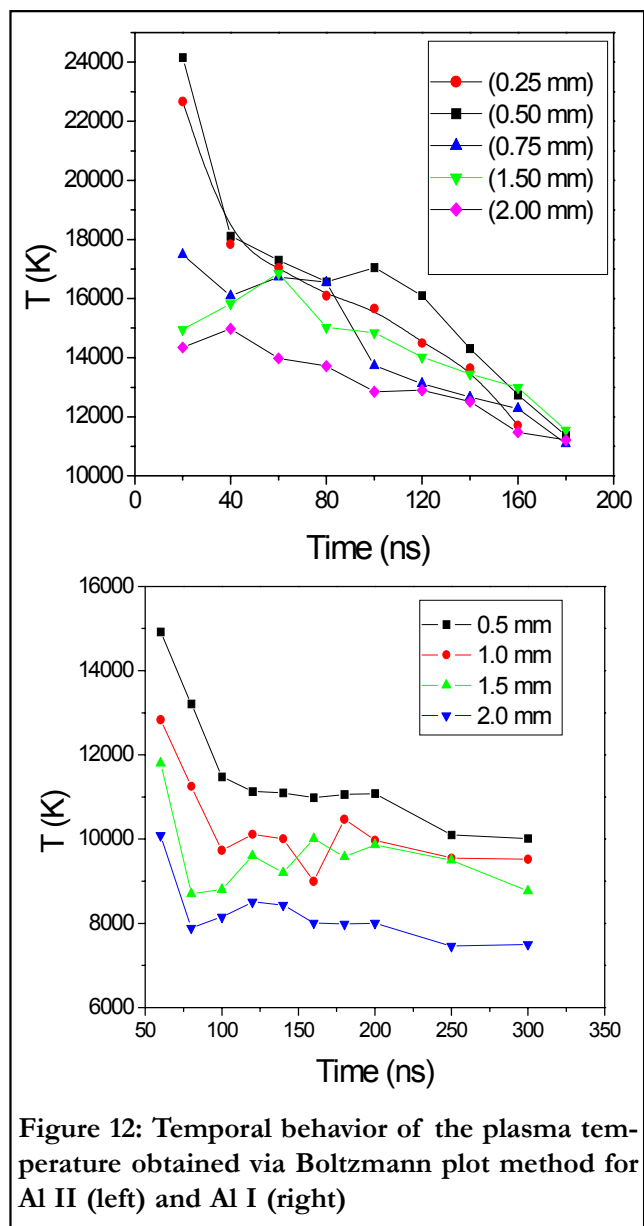


Figure 12: Temporal behavior of the plasma temperature obtained via Boltzmann plot method for Al II (left) and Al I (right)

down, radiative processes such as spontaneous emission, reabsorption and stimulated emission are predominant over the collisional effects, thus invalidating the LTE approximation.

In the same way, at longer distances from the target the electron density in the plasma is low, so that the thermal equilibrium between the plasma species cannot be sustained by the electron-ion collisions. At low values of the electron density the three-body recombination effect has also to be taken into account. All these effects lead to the violation of the LTE approximation, thus giving apparently different plasma temperatures when considering the

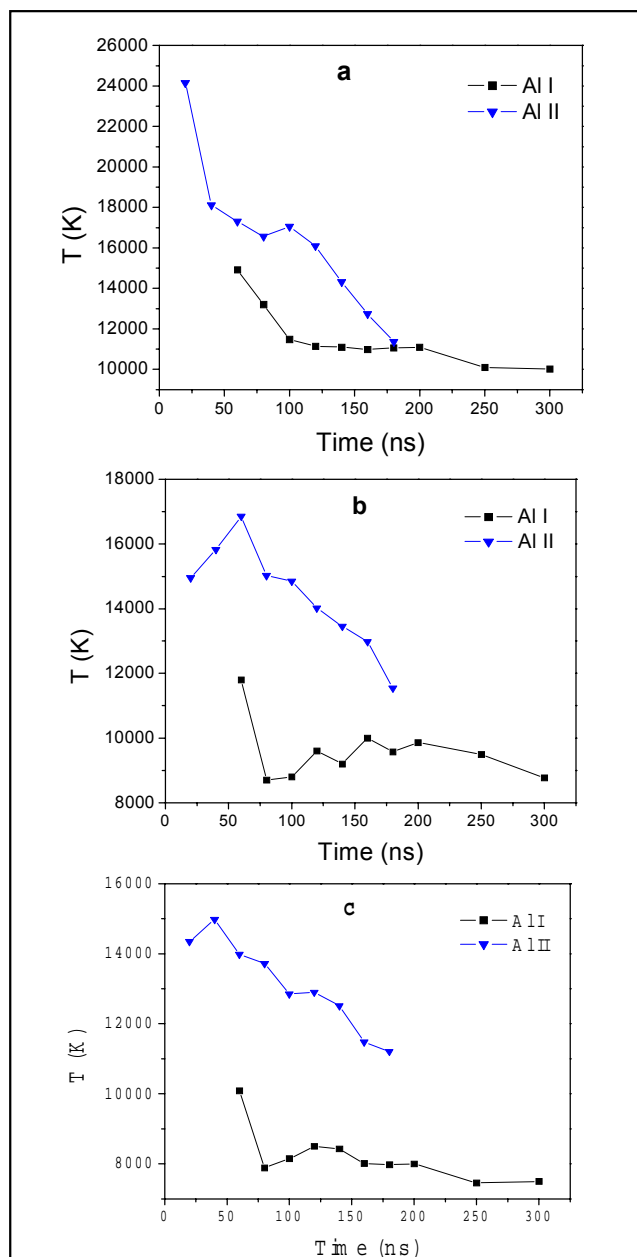


Figure 13: Time dependence of the plasma temperature calculated via Boltzmann plot method for Al I and Al II at (a) 0.5 mm from the surface; (b) 1.5 mm from the surface; (c) 2 mm from the surface

different species in the plasma.

## CONCLUSION

In this work, we have reported experimental results on the dynamics of laser-induced plasmas in vacuum. The thermodynamical properties of the

plasma, as well as its composition have been studied using the optical emission spectroscopy (OES) technique, involving high-resolution broadband detection of the plasma optical emission with high temporal and spatial resolution. Using the optical Time of Flight (TOF) technique, the expansion velocity of the laser-induced plasma was measured in vacuum. The analysis of the plasma optical emission also facilitated the measurement of time and spatial profiles of plasma electron density and temperature during the plasma expansion stage.

Moreover, modeling and theoretical analysis of the experimental data allowed the study of non-equilibrium processes in the laser-induced plasmas. Investigation of the plasma expansion in vacuum, revealed a departure from equilibrium which has been explained in terms of the three-body recombination effect. The corresponding rate constant of such effect  $k_{rec}$  was measured. The obtained results were in good agreement with the corresponding theoretical estimates.

Finally, deviations from the Saha balance were found. An explanation of the phenomenon was given in terms of radiative effects and three-body recombination too.

#### ACKNOWLEDGMENT

The authors would like to thank Dr.A.De Giacomo for the very useful discussions and con-

structive advices.

#### REFERENCES

- [1] 1<sup>st</sup> International conference on laser induced plasma spectroscopy and applications, Tirrenia, Pisa, Italy, October 8-12, (2000), *Spectrochim.Acta Part B*, **56**, 6 (2001).
- [2] 1<sup>st</sup> Euro-Mediterranean Symposium on laser induced breakdown spectroscopy, Cairo, Egypt, November 2-6, (2001), *Spectrochim.Acta Part B*, **57**, 7 (2002).
- [3] 2<sup>nd</sup> International conference on laser induced plasma spectroscopy and applications, Orlando, Florida, USA., September 25-28, OSA Trends in optics and photonics (2002).
- [4] 2<sup>nd</sup> Euro-Mediterranean Symposium on laser induced breakdown spectroscopy, Hersonissos, Crete, Greece., 30 September, 3 October (2003), *J.Anal. Atomic Spectrometry*, **19**, 4 April (2004).
- [5] M.Capitelli, A.Casavola, G.Colonna, A.De Giacomo; *Spectrochim.Acta Part B*, **59**, 271 (2004).
- [6] J.Herman, C.Boulmer-Leborgne, D.Hong; *J.Appl. Phys.*, **83**(2), 691 (1998).
- [7] H.R.Griem; 'Principles of Plasma Spectroscopy' Cambridge University Press, (1997).
- [8] J.A.M.Van der Mullen; *Physics Reports of Physics Letter, PRPLCM*, **191**(2 and 3), 109 (1990).
- [9] S.Amoruso, R.Bruzzese, N.Spinelli, R.Velotta; *J.Phys., B, At.Mol.Opt.Phys.*, **32**, R131-R172 (1999).
- [10] A.De Giacomo, V.A.Shakhatov, O.De Pascale; *Spectrochim.Acta, B*, **56**, 753 (2001).
- [11] A.De Giacomo; *Spectrochim.Acta, B*, **58**, 753 (2003).
- [12] D.A.Cremers; *Appl.Spectrosc.*, **41**, 572 (1987).
- [13] R.Noll, H.Bette, A.Brysch, M.Kraushaar, L.Monch, L.Peter, V.Sturm; *Spectrochim.Acta, B*, **56**, 637 (2001).
- [14] S.Rosenwasser, G.Asimellis, B.Bromley, R.Hazlett, J.Martin T.Pearce, A.Zigler; *Spectrochim.Acta B*, **56**, 707 (2001).
- [15] M.Capitelli, F.Capitelli, A.Eletskii; *Spectrochim.Acta B*, **55**, 559 (2000).
- [16] W. Sdorra, K.Niemax; *Microchim.Acta*, **107**, 319 (1992).
- [17] H.R.Griem; 'Plasma Spectroscopy' McGraw-Hill, New York, (1964).
- [18] NIST Atomic Spectra Database. Available from [www.physics.gov](http://www.physics.gov).
- [19] L.J.Radziemski, D.A.Cremers, T.R.Loree; *Spectrochim.Acta B*, **38**, 349 (1983).